ADVANCED SUSTAINABLE SYSTEMS
www.advsustainsys.com

Mid-Infrared Spectroscopy and Machine Learning for Nondestructive Detection of Inapparent Deterioration in Acrylic Waterborne Coatings for Wood

Yoshikuni Teramoto, Takumi Ito, Chihiro Yamamoto, Toshiyuki Takano, and Hironari Ohki*

This study presents an approach for nondestructive detection of inapparent deterioration in waterborne acrylic coatings (containing cellulose nanofibers (CNFs)) for wood by using mid-infrared spectroscopy and machine learning. The method evaluates films that mimic coatings before and after 500 h of accelerated weathering, equivalent to roughly 1 year of outdoor exposure. No noticeable transformation in film appearance is evident with a spectrophotometer following the accelerated weathering. Chemiluminescence analysis indicates oxidative degradation predominantly in the acrylic resin, an impact that the CNFs seem to mitigate. Whereas attenuated total reflectance (ATR)-Fourier transform infrared (FTIR) spectroscopy commonly identifies chemical changes in visibly degraded coatings, it does not clearly discern prior, inapparent deterioration. In this context, machine learning algorithms (such as *k*-nearest neighbors, decision tree, random forest (RF), and support vector machine (SVM)) categorize these nuanced changes by using the absorbance from 400 to 4000 cm^{-1} as explanatory variables. The SVM model exhibits the highest predictive accuracy, and the RF recognizes crucial variables in some wavenumber zones. This approach has the potential for enhancing recoating schedules, cutting costs, and encouraging sustainable use of wood.

1. Introduction

Wood coatings are widely used because they are relatively inexpensive and effective in protecting as well as adding aesthetic appeal to woody materials.[1–3] In recent years, the increasing demand for sustainable products has led to a worldwide increase in the number of medium- and high-rise wooden buildings[4]; thus the importance of wood coatings should increase. However, in general, long-term deterioration of coating barrier properties is not fully understood, and its elucidation continues to be of substantial scientific and industrial interest.[5]

Regarding coated wood, chemical and physical degradation of the coating causes pinholes, cracks, or scratches that rapidly progress the biological degradation of the wood (cell wall degradation initiated by bacteria and fungi).[6] It is therefore important to extend the period that precedes deterioration and learn how to predict it. However, current evaluation methods[7] mainly use apparent indicators that manifest during deterioration (such as cracks, blisters, and peeling of the paint film) and comparisons of discoloration as well as fading with product samples. It is thus difficult to obtain information on preliminary (inapparent) stages before apparent deterioration. If it is possible to quickly and nondestructively diagnose chemical deterioration of wood coatings at a stage that cannot be visually recognized, one can then determine an appropriate timing for recoating to prevent biodegradation. Thus, maintenance costs can be reduced in the long term. It will furthermore be possible to utilize wood in a carbon-fixed state for an extended period, contributing to the achievement of goals 12 (ensure sustainable consumption and production) and 15 (sustainably managed forests) of the United Nations' Sustainable Development Goals.

In this study, we devised a method that combines infrared spectroscopy and machine learning (classification) to propose a nondestructive deterioration diagnosis method for wood coatings at a stage that cannot be visually recognized. We herein applied accelerated weathering treatment (xenon lamp method[7]) to film specimens that approximated wood coatings for outdoor structures. The treatment time was 500 h, which corresponds to ≈1 year of outdoor exposure. Beforehand and afterward, we obtained attenuated total reflectance (ATR)-Fourier

Y. Teramoto, C. Yamamoto, T. Takano
Division of Forest and Biomaterials Science, Graduate School of Agriculture
Kyoto University
Kitashirakawa Oiwake-cho, Sakyo-ku, Kyoto 6068502, Japan
E-mail: teramoto.yoshikuni.3e@kyoto-u.ac.jp
T. Ito, H. Ohki
Gen Gen Corporation
74 Aza Nakano Ori, Kamori-cho, Tsushima city, Aichi 4960005, Japan
The ORCID identification number(s) for the author(s) of this article can be found under https://doi.org/10.1002/adsu.202300354

DOI: 10.1002/adsu.202300354

transform infrared (FTIR) spectra in the mid-infrared region (400–4000 cm^{-1}), totaling 109 spectra. Compared to the big data machine learning that has caused a global boom in the past decade, this is small-scale data. Only recently, machine learning for small-scale chemical data has gained attention due to the low cost of data acquisition and advancements in machine learning techniques.[8]

On the other hand, research on machine learning of spectra, particularly in the field of plastic recycling, has been increasing significantly in recent years.[9–11] Meanwhile, in order to evaluate degradation for coatings, many studies have focused on changes in specific bands in the mid-infrared spectrum.[5,12–19] However, to our best knowledge, there is no example of analyzing the spectrum of the entire wide mid-infrared region for coating films by using modern statistical methods. A method for diagnosing coating embrittlement by multivariate analysis of the near-infrared spectrum has been patented.[20] However, because the molar extinction coefficient in the mid-infrared region is on the order of 10^3 times that in the near-infrared region and has high sensitivity, we hypothesized that it might be suitable for detecting inapparent changes. Moreover, the ATR method has the advantage of being applicable to the maintenance of buildings that have already been constructed because the data acquisition cost is low and some corresponding devices are portable.[21] We herein applied several classification machine learning techniques to the spectral data with the aim of determining whether the film specimens had undergone accelerated weathering. We also subjected the coating film specimens to spectrophotometric and chemiluminescence analysis (CLA) to obtain additional information on accelerated weathering.

We prepared the coating film specimens with formulations corresponding to waterborne acrylic resin emulsion (latex) paints for exterior wood. The series of specimens contained cellulose nanofibers (CNFs) in various proportions. Adding CNFs to wood coatings has the effect of controlling the surface gloss of painted wood as well as suppressing surface defects and discoloration.[22] Because paint generally contains additives, the study design also included a feasibility evaluation to determine the deterioration of the film specimens with various formulations.

2. Experimental Section

2.1. Preparation of CNFs

CNFs were produced by subjecting Japanese cedar chips (*Cryptomeria japonica* D. Don) from Gifu Prefecture (Japan) to soda–anthraquinone cooking and bleaching, followed by defibrating by enzymatic treatment as well as wet grinding.[22,23] Briefly, an aqueous suspension of pulp was prepared to 2.4 wt.%, and cellulase XL-531 (genus *Aspergillus*, Nagase ChemteX) was added: 5 mg of enzyme per 1 g of pulp. LMZ2 (Ashizawa Finetech) was used as a bead mill, 85% of the chamber was filled with zirconia beads (diameter: 1 mm), and the peripheral speed was 12 m s^{-1}. The final CNF aqueous dispersion had a solids concentration of 2.4 wt.%. The average length and width were 682 and 41 nm, respectively. These dimensional values are the average of 100 fibers observed by transmission electron microscopy. This CNF contained ≈20% hemicellulose per dry weight.

2.2. Preparation of CNF-Containing Film Specimens

In reference to the formulations of commercial outdoor wood coatings, analogous film specimens with various CNF contents were prepared based on waterborne acrylic resin emulsions (latexes). The aqueous acrylic resin emulsions NeoCryl XK-190 (acrylic resin 1) and XK-12 (acrylic resin 2) from Covestro AG were mixed with the CNF aqueous dispersion, antifungal agent, preservative, UV absorber, and defoamer. Film specimens with a thickness of 100 μm were prepared by repeatedly spraying the mixture onto a release sheet and drying the sheet in a blower dryer at 50 °C. **Table 1** shows the formulations of the films prepared in this study.

2.3. Accelerated Weathering Treatment (Xenon Lamp Method)

Accelerated weathering treatment (xenon lamp method) assuming outdoor use was performed with a weather resistance tester XER-W83 (xenon tester, Iwasaki Electric) in accordance with Japanese Industrial Standards (JIS) K 5600-7-7:2008.[7] Prior to the treatment, the films were cut to 140 mm × 65 mm while still attached to the release sheet. The treatment was carried out for 500 h at an irradiance of 60 W m^{-2} (300–400 nm) under the spectral distribution of the UV–vis regions of the horizontal plane, all-sky radiation. The black panel temperature was 63 ± 2 °C. During treatment, a cycle of 18 min wetting time and 102 min drying time was conducted under continuous irradiation. The relative humidity during the drying period was 50% ± 5%.

2.4. Gloss and Color Coordinate Measurements

A CM-26d (Konica Minolta, Inc.) was used as a digital spectrophotometer. A CR-A43 calibration plate (Konica Minolta) was used as a white calibration plate and background during the measurements. A D65 light source specified by the International Commission on Illumination (CIE) was used; the illumination aperture was set to 8 mm. An 8° gloss was measured as an index of the gloss of the films. This is a manufacturer's standard that approximates the glossiness formulated in JIS Z 8741, in which the specular reflectance of a glass surface with a refractive index of 1.567 corresponds to a glossiness of 100. The calculation is by obtaining the spectral regular reflectance in the 8° direction, from the difference between the spectral total reflectance and the spectral diffuse reflectance in the optical system of the spectrophotometer, and integrating the result over the wavelength. The color coordinates defined by the CIE (L^*, lightness; a^*, redness; b^*, yellowness) were also measured with the digital spectrophotometer. A colorimetric method was used, termed specular component excluded, which excludes specular reflectance. For the measurements, the films that had undergone accelerated weathering and those that had not (as-prepared) were used. Five measurements were recorded for each specimen. Based on L^*, a^*, and b^* of the as-prepared CNF0 specimen, the color difference ΔE^*_{ab} was calculated as the square root of the sum of squares of the difference from those coordinate values of the other specimens.

Table 1. Composition of acrylic resin-based films containing cellulose nanofibers (CNFs). Numerical values indicate weight percentages in the dry state.

Specimen Code	Acrylic Resin 1 (XK-190)	Acrylic Resin 2 (XK-12)	Antifungal Agent	Preservative	UV Absorber	Defoamer	CNF	Total
CNF0	43.7	43.7	0.8	0.2	9.7	1.9	0	100
CNF1.2	42.4	42.2	0.8	0.2	9.5	1.9	1.2	100
CNF3.8	42.0	42.0	0.7	0.2	9.3	1.9	3.8	100
CNF12.7	38.1	38.1	0.7	0.2	8.5	1.7	12.7	100
CNF17.5	36.1	36.1	0.6	0.2	8.0	1.5	17.5	100
CNF24.9	32.9	32.9	0.5	0.1	7.3	1.4	24.9	100
CNF44.5	25.0	25.0	0.2	0.1	4.1	1.0	44.5	100

2.5. CLA

By using a chemiluminescence spectrometer (CLA-FS4, Tohoku Electronic Industrial) equipped with a CLS-SH1 as a chamber, chemiluminescence (CL) measurements were performed from 50 to 250 °C under a nitrogen flow of 100 mL min^{-1}. The heating rate was 20 °C min^{-1}. The weather-treated and as-prepared films were cut to 10 mm × 10 mm and used for the measurements. Peroxides (assumed to be formed during accelerated weathering) were thermally decomposed, and CL (emitted from excited carbonyls) was detected as the number of photons integrated over 1 s with a photomultiplier. The first peak during the temperature increase corresponds to the quantity of peroxide.

2.6. Mid-Infrared Spectroscopy

An FTIR spectrophotometer Spectrum3 (PerkinElmer), equipped with a universal ATR accessory (KRS-5/diamond), was used to measure the spectra of specimens before and after accelerated weathering. The wavenumber range was 400–4000 cm^{-1} (number of accumulations: 16; wavenumber resolution: 4 cm^{-1}). The obtained absorbance spectra were subjected to ATR correction with instrument control software, and the absorbance at 1159 cm^{-1} was normalized to 1.

2.7. Data Analysis and Software: Building and Testing Classification Models

ATR–FTIR spectra were measured >3× for the as-prepared and weathered specimens with eight CNF contents, and a total of 109 spectra were acquired. Using the normalized absorbance at 1 cm^{-1} intervals from 400 to 4000 cm^{-1} and the CNF content in the coating film as explanatory variables, models were constructed and verified that classified the films as either as-prepared or weathered. The dataset was randomly split into training data for building the classification model (44 samples) and test data (20 samples) for verifying the model's estimation performance.

The classification models were implemented in Python 3.9.12 (Python Software Foundation, Wilmington, DE, US). The programs *k*-nearest neighbor (*k*-NN) algorithm,[24] decision tree (DT),[25] random forest (RF),[26] and support vector machine (SVM)[27] methods (published in Dr. Hiromasa Kaneko's book[28] and repository[29]) were modified and used. Hyperparameters that need to be determined in advance for classification model construction were determined in principle by cross-validation. The Supporting Information summarizes each concept and implementation procedure.

The classes of both the training and test data were known in the samples used in this study, but the classes of the test data were blinded. After estimating the class of the test data, the answers were checked by using the correct class. To check the answers efficiently, a table was created to summarize the results of classification, termed a confusion matrix. The accuracy rate, which is an index for quantitatively evaluating the estimation results of the classification model, was calculated by dividing the number of correctly classified samples by the total number of samples.

3. Results and Discussion

3.1. Visual Observation and Spectrophotometric Colorimetry of Film Specimens

Visual observation and spectrophotometric colorimetry were performed to quantify the apparent effects of weathering on the CNF-containing film specimens that approximate the exterior coating of wood. **Figure 1** shows photographs acquired through an 8 mm aperture of the surface of the series of specimens and colorimetric data.

For all specimens, the grade for indicating the size of coating film cracks in JIS K 5600-7[7] corresponded to grade 0. Thus, there were no visible cracks after weathering, even upon 10× magnification. The 8° gloss value of specimens generally decreased with increasing CNF content (Figure 1b). The effect of the weathering on the gloss was not clear. We observed yellowing with increasing CNF content in the as-prepared specimens (Figure 1a). Correspondingly, the color difference ΔE^*_{ab} (Figure 1c) also increased with CNF content. However, in the weathered specimens, $\Delta E^*_{ab} = 3.56$ for CNF0; and even if the CNF content increased, the value was equal to or slightly higher than that value and did not increase monotonically. Cellulose and hemicellulose in CNF are known to produce yellow-brown colored substances when their reducing end groups of the polysaccharide chains rapidly react to heat, as reported by Kawamoto et al.[30] These colored materials can be extracted using water. In our process of preparing CNF-containing film specimens, we conducted forced air drying at 50 °C. It is believed that the coloring substances were formed during this drying phase, and these were likely eluted and lost by water spraying during the accelerated weathering.

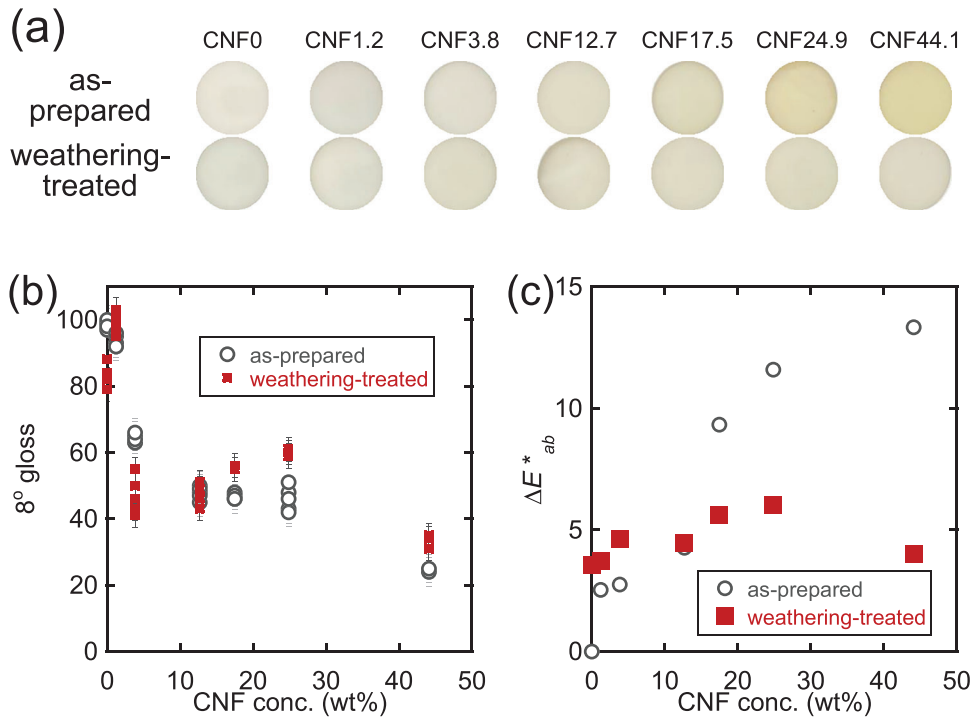

Figure 1. Appearance of as-prepared and weathering-treated film specimens and their colorimetric data: a) photographs obtained through an 8-mm aperture, b) 8° gloss, and c) color difference ΔE^*_{ab} based on that of as-prepared CNF0.

The effect of the weathering on the appearance was thus unclear. In other words, even if the weathering had an effect on the film specimens, the changes were not visually evident.

3.2. CLA

CLA was used to evaluate the oxidative degradation of the specimens. The photomultiplier built into the CLA apparatus can detect weak luminescence on the order of tens of photons.[31] In the autoxidation mechanism of organic polymers,[31–33] unoxidized polymers generate radicals when stimulated by light or heat; these radicals react with oxygen in the air to generate peroxy radicals (ROO·) and then peroxides (ROOH). ROOH decomposes into ROO·, and the reaction between the two radicals produces excited carbonyl as well as singlet oxygen with high energy states. When these substances return to the ground state, they release energy as light and heat. By detecting the weak light generated at that time, the quantity of ROOH formed (the degree of oxidation degradation of the specimen) can be measured as the quantity of light emitted.

In this study, by heating as-prepared or weathered film specimens, the small quantity of ROOH (assumed to have formed and accumulated in the specimen) decomposed, and we measured the resulting chemiluminescence (CL). **Figure 2** shows the time course of CL generated from CNF0 and CNF12.7. For both systems, we observed a clear peak (marked with a red arrow) ≈300 s, corresponding to ≈150 °C in the weathered specimens, but almost no peak was evident in that temperature region for the as-prepared samples. Comparing the weathered samples with each other, although the acrylic resin content in the CNF12.7 specimen was 0.87× that of CNF0, the CL peak intensity was reduced by less than half. Thus, the weathering oxidized mainly the acrylic resin component of the specimen in a manner that produced peroxides. Adding CNFs might have suppressed oxidative degradation of the acrylic resin matrix.

In general, carbonyls derived from oxidation products that are detectable by CLA can be identified by mid-infrared spectroscopy only after accumulation to a considerable extent.[31] High-sensitivity CLA was thus useful for detecting inapparent (oxidative) deterioration of the film specimens in this study. However, CLA is not suitable for onsite application because it requires special equipment that is not usually portable and is not a nondestructive testing method.

3.3. ATR–FTIR and Classification

3.3.1. Evaluating the Effects of Weathering

The literature reports chemical changes in the oxidation of waterborne acrylic coatings by heat and light have been investigated by FTIR spectroscopy.[12,13] **Figure 3**a shows the typical changes because of the formulation and weathering treatment of the CNF-containing acrylic coating films in this study. For reference, a set of spectra with ATR correction and intensity normalization at 1159 cm^{-1} are shown in Figures S1 and S2 (Supporting Information). We normalized the intensity of those spectra by the band intensity at 1159 cm^{-1}, considered to be negligible during photooxidation of the acrylic resin coating.[12] In terms of the formulation, increasing CNF content resulted in two major increases in intensity of the OH stretching vibration, with a maximum at

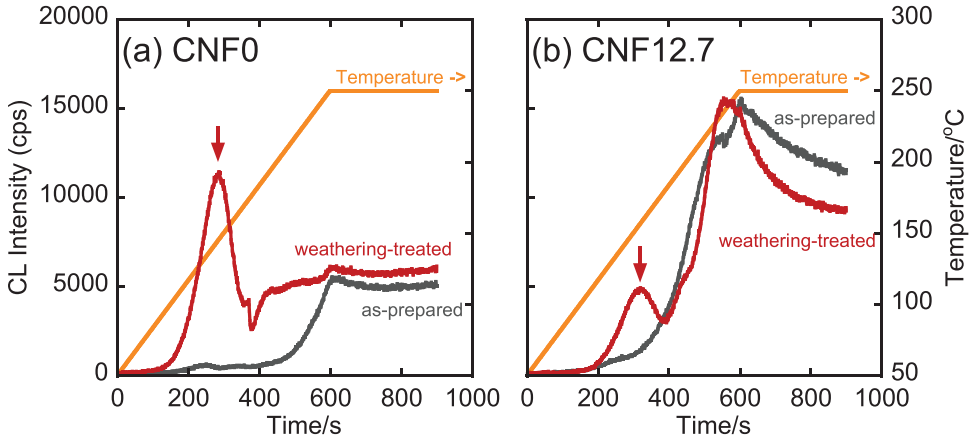

Figure 2. Time course of chemiluminescence measurements with heating from 50 to 250 °C at 20 °C min^{-1} and holding for 5 min, under nitrogen: a) CNF0 and b) CNF12.7. We subjected the film specimens (as provided (red line) and weathered (gray line)) to the measurements. The orange line refers to the temperature change as labeled on the right-hand axis.

≈3340 cm^{-1} as well as the C–O stretching vibrations of ethers and alcohols ≈1050 cm^{-1}.

Figure 4a shows an enlarged view from 900 to 1800 cm^{-1} wavenumber region of Figure 3a. Several bands in the FTIR spectra of acrylic resins change in association with photo-oxidation. Such changes occur when a resin is exposed to harsh conditions:, e.g., after thousands of hours of continuous irradiation with a 500 W, high-pressure mercury–tungsten lamp (wavelength >300 nm, 50 °C, and ambient relative humidity).[12] These changes have been interpreted in the literature as follows[12]: i) broadening and decreasing intensity of the carbonyl band at ≈1730 cm^{-1} (cleavage because of decomposition of the ester side chain), ii) development of a shoulder at ≈1780 cm^{-1} (formation of γ-lactone), and iii) manifestation of a weak absorption band at 1640 cm^{-1} (terminal carbon–carbon unsaturations are produced as a consequence of chain scission).

However, it was recognized that the 500 h of weathering by the xenon lamp method introduced in our study constitutes relatively mild photo-oxidation conditions compared to the severe conditions mentioned in ref.,[5] thus it was anticipated that explicit changes in the carbonyl bands would not be observed. This informed our approach of integrating machine learning to detect subtle, non-explicit transformations and patterns in the spectral data that may not be immediately discernible. Consequently, it was difficult to observe the changes in (i) and (ii) in the spectra of the film specimens, which we subjected to 500 h of weathering by the xenon lamp method. Regarding the band near 1640 cm^{-1} related to (iii), we could not identify the change before and after weathering for CNF0, but there seemed to be a difference for specimens containing CNFs.

We performed classification by *k*-NNs, DT, RF, and SVM to identify inapparent changes in the film specimens because of weathering. The explanatory variables are the CNF content in the specimen and the normalized absorbance of the ATR–FTIR spectra from 400 to 4000 cm^{-1} in 1 cm^{-1} steps. Here, the objective variable was to classify into two classes: as-prepared and weathered. We used ≈70% of the sample's training data to create a classification model and tested the remaining ≈30% of the samples.

In **Figure 5**, we present the learning curves for the respective classifiers, namely a) *k*-NN, b) DT, c) RF, and d) SVM. These curves plot both the training and test accuracy, starting from ten randomly selected samples, incrementing in steps of 5, and culminating at 109 samples. Additionally, we have incorporated rates of false negatives and false positives concerning the test data into these curves. To elaborate, false negatives pertain to samples genuinely categorized as "weathering-treated" but were predicted as "as-prepared," and false positives represent samples genuinely identified as "as-prepared" but predicted as "weathering-treated."

Drawing insights from these learning curves, we observed the following trends:

(a) The *k*-NN classifier exhibited a consistently low accuracy rate across both training and test data sets. Notably, the crucial false negative rate remained ≈0.5, even when the sample count exceeded 100, rendering it unsuitable for practical applications.

(b) For the DT classifier, the training data's accuracy hovered ≈0.9, and the test data exhibited ≈80% accuracy. The rate of false negatives did not diminish below ≈0.2.

(c) The RF classifier showcased near–perfect accuracy, close to 1, for the training data regardless of the sample size. Beyond a sample count of 40, test data accuracy predominantly ranged between 0.8 and 0.9. The false negative rate showed a gradual decline, yet persisted ≈0.2 even with samples exceeding 100.

(d) Similar to RF, SVM's training data accuracy was ≈1 across all sample sizes. Test data accuracy frequently surpassed 0.9 when the total samples exceeded 60. The false negative rate was generally ≈0.1, although there were some results where the rate was high.

While it is conceivable that enhancing the sample size might further elevate the test data accuracy, the SVM, which appears to be converging to a false–negative rate ≈0.1, is deemed most apt for constructing prediction models with this dataset's magnitude.

In Figures S3 and S4 (Supporting Information), we present the complete set of spectra that have been normalized solely at

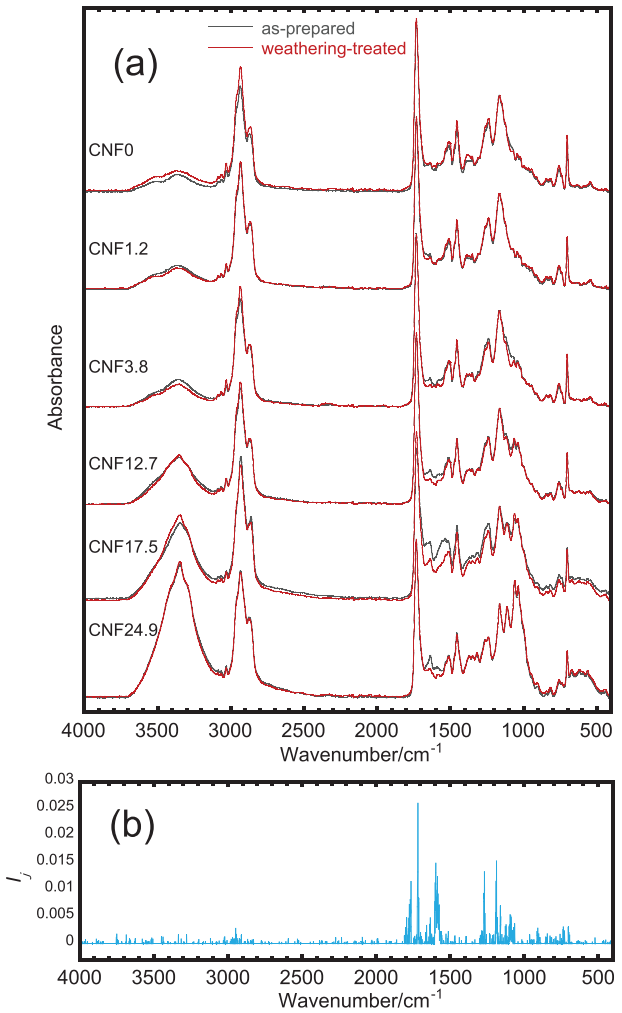

Figure 3. a) ATR–FTIR spectra of as-prepared as well as weathering-treated film specimens with various cellulose nanofiber (CNF) contents. The spectra shown here have been ATR-corrected using the software provided with the measurement device and then normalized to an absorbance of 1 at the 1159 cm^{-1} band intensity. b) Importance I_j of explanatory variables (wavenumbers) in classification by random forest in the same wavenumber range (The number of samples in this dataset was 109.).

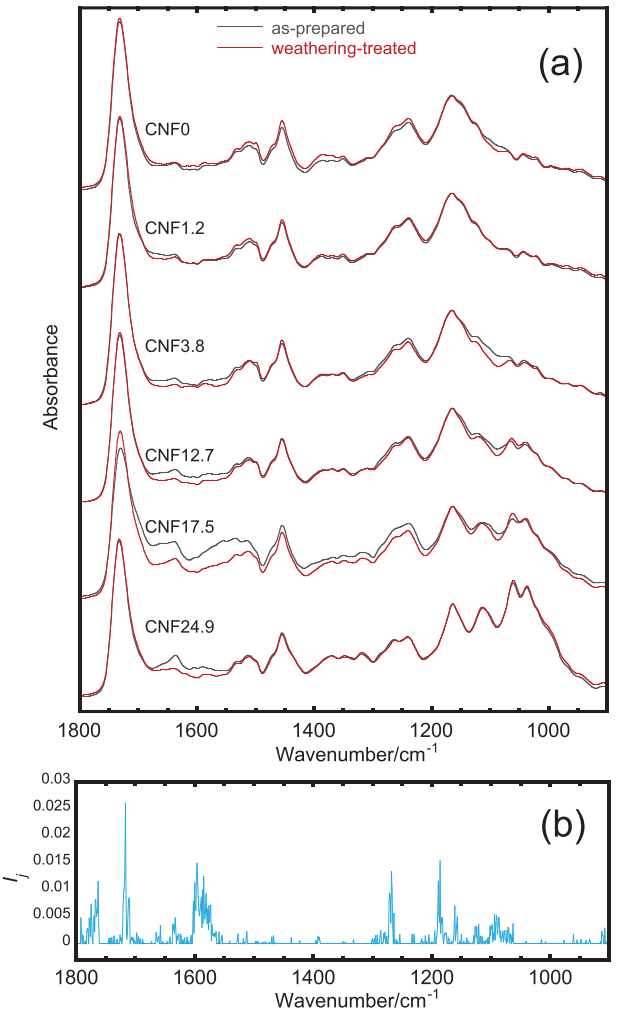

Figure 4. a) Magnified view of 900–1800 cm^{-1} of ATR–FTIR spectra of as-prepared as well as weathered film specimens with various cellulose nanofiber (CNF) contents, and b) importance I_j of explanatory variables (wavenumbers) in classification by RF in the same wavenumber range (The number of samples in this dataset was 109.).

the intensity of 1159 cm^{-1} without ATR correction. Furthermore, the learning curves are illustrated in Figure S5 (Supporting Information). While these curves exhibited a trend similar to those in Figure 5, which underwent ATR correction, the SVM's training data accuracy and false negative rate were lower.

3.3.2. Evaluation of Importance of Explanatory Variables (Wavenumber) by RF

RF can quantify the importance of explanatory variables I_j (Equation S2, Supporting Information).[26,28] For an explanation of I_j, see the section on "Variable importance in a RF model" in Supporting Information. Below the absorbance spectra in Figure 3a and Figure 4a, Figure 3b and Figure 4b show the I_j data in the corresponding wavenumber regions. In the plot of I_j in Figure 3b, we observed no region with large values from 2000 to 4000 cm^{-1}, indicating that the importance of that wavenumber region was low for RF classification under this condition.

It should be noted that there was no systematic decrease in the intensity of the ester carbonyl band peaking at 1730 cm^{-1} (Figure 4a), but the I_j value was high in the regions flanking the peak (Figure 4b). In particular, the low wavenumber side of the peak exhibited the maximum I_j value in the entire wavenumber region. This suggests that the RF was identifying changes in the broadening of the C=O stretching band from the acrylic resin's ester. Such changes might be linked to alterations in this band area of the acrylic resin, potentially due to oxidative degradation from significant light exposure as previously discussed.

The wavenumber region in which another I_j was large is the region from 1550 to 1600 cm^{-1}. We thus also considered this wavenumber region to be of high importance for classification. This wavenumber region generally corresponds to absorbance attributable to C=C stretching vibrations. As-prepared specimens

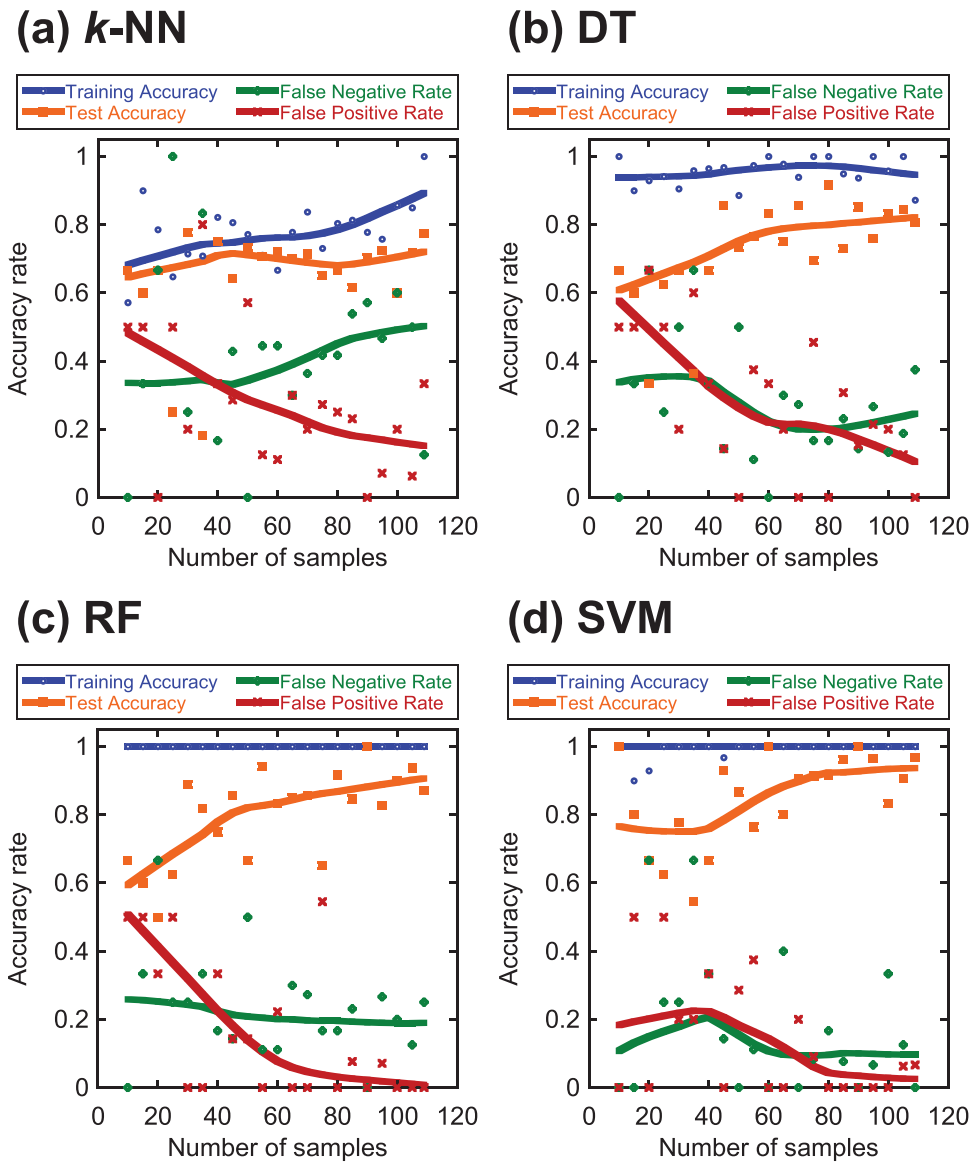

Figure 5. Learning curves for a) *k*-nearest neighbors (*k*-NN), b) DT, c) RF, and d) SVM, based on the statistical processing of ATR–FTIR spectra that underwent ATR correction and were normalized at the 1159 cm^{-1} band intensity. The curves depict the evolution of training and test accuracy, starting from a sample size of 10 and increasing in increments of 5. Also shown are the rates of false negatives and false positives for the test data, which represent instances incorrectly predicted as "as-prepared" and "weathering-treated", respectively. Each plot's regression curve is generated using the "Weighted" method in KaleidaGraph Version 4.1.1, with a smoothing coefficient of 66%.

with a high CNF content exhibited increased absorbance in this region, suggesting that C=C might be formed not only on the acrylic resin but also on the cellulose side. Moreover, in the CNF-containing system, the uptake of absorption at 1500–1700 cm^{-1} tended to decrease after weathering. This might correspond to the spectrophotometric data and the observation that yellowing was prominent in the as-prepared specimens but was no longer evident in the weathered specimens. In other words, the component that caused yellowing might have an absorption in this band region.

From 1000 to 1300 cm^{-1} (corresponding to the absorbance of the C–O stretching vibrations of esters, ethers, and alcohols), it was difficult to discern systematic changes in the spectrum itself in Figure 4a. However, we observed some local maxima for I_j. This suggests that there was some change in the structure associated with this region.

In Figure S6 (Supporting Information), we present the plot of I_j for the dataset without ATR correction. Even without the ATR correction, peaks were observed in the wavenumber regions where I_j values were high when ATR corrected, both s of the peak at 1730 cm^{-1} and the region between 1550 and 1600 cm^{-1}. However, the peaks indicated by I_j were generally sharper.

Accordingly, one might be able to classify the effects of weathering on film specimens that approximate wood coatings by combining mid-infrared spectroscopy and machine learning, even if the compounding ratios differ.

3.3.3. Applicability to Actual Systems

For our model film specimens in this study, a film thickness of 100 μm was chosen. Even though this is considerably thicker than the standard 30 μm observed in waterborne coatings for wood, there is a specific reason behind our decision. The selection is based on the penetration depth of the evanescent wave during our ATR–FTIR experiments. When using KRS-5/diamond as internal reflection elements at an incident angle of 45° within the wavenumber range of 400–4000 cm^{-1}, the penetration depth of the evanescent wave is consistently between ≈0.5 and 5 μm. Notably, at sensitive wavenumbers between 1000 and 1800 cm^{-1}, the depths range from ≈1.1 to 2.0 μm, which is less than the standard thickness of wood coatings. This ensures our findings hold relevance to real-world applications.

Existing portable hand-held ATR–FTIR devices[21] offer promise for on-the-spot assessments of coating surfaces on wooden structures already in use. A major advantage lies in the absence of a need for specialized spectral processing; ATR correction and intensity normalization alone are required, both standard features in the software of these devices. The methodology proposed in this study may be key to uncovering the "invisible deterioration" of acrylic waterborne coatings on wood. While not conceptualized as an automatic monitoring tool for coated wood, its applicability spans to real-world, including sizeable, wooden constructs.

4. Conclusion

This study presents a method for nondestructive evaluation of inapparent deterioration in wood coatings by using infrared spectroscopy combined with machine learning. Our findings reveal that CNFs can mitigate oxidative degradation caused by the weathering of acrylic resins. However, the changes are not easily visible and hence require specialized techniques to discern. Several machine learning algorithms (including *k*-NNs, DT, RF, and SVM) classified these changes. SVM achieved the highest predictive accuracy. The RF model detected important features in various wavenumber regions. Thus, this research offers a foundation for applying mid-infrared spectroscopy and machine learning to detect as well as analyze the effects of weathering on wood coatings, regardless of their compounding ratios. Our future research will focus on regression analysis, which will better serve diagnostic purposes compared with classification, thereby contributing to the field of wood coating maintenance and conservation.

Supporting Information

Supporting Information is available from the Wiley Online Library or from the author.

Acknowledgements

The authors express sincere gratitude to Mr. Ryota Samejima of Tohoku Electronic Industrial for gracious assistance and provision of the CLA instrumentation. The authors gratefully acknowledge the support from the Japan Science and Technology Agency (JST) under the Adaptable and Seamless Technology Transfer Program through Target-driven R&D (A-STEP), grant number 22682848. This work was also partly supported by JSPS KAKENHI Grant Number 21H02256. The authors thank Michael Scott Long, Ph.D., from Edanz (https://jp.edanz.com/ac) for editing a draft of this manuscript.

Conflict of Interest

The authors declare no conflict of interest.

Data Availability Statement

The data that support the findings of this study are available from the corresponding author upon reasonable request.

Keywords

accelerated weathering, cellulose nanofibers, inapparent deterioration, machine learning, mid-infrared spectroscopy, nondestructive detections, waterborne acrylic wood coating

Received: August 8, 2023
Revised: October 21, 2023
Published online: November 8, 2023

[1] R. S. Mohd Ghani, *Prog. Org. Coat.* **2021**, *160*, 106523.
[2] A. Dorieh, M. Farajollah Pour, S. Ghafari Movahed, A. Pizzi, P. Pouresmaeel Selakjani, M. Valizadeh Kiamahalleh, H. Hatefnia, M. H. Shahavi, R. Aghaei, *Prog. Org. Coat.* **2022**, *165*, 106768.
[3] L. Dall Agnol, F. T. G. Dias, H. L. Ornaghi, M. Sangermano, O. Bianchi, *Prog. Org. Coat.* **2021**, *154*, 106156.
[4] M. H. Ramage, H. Burridge, M. Busse-Wicher, G. Fereday, T. Reynolds, D. U. Shah, G. Wu, L. Yu, P. Fleming, D. Densley-Tingley, J. Allwood, P. Dupree, P. F. Linden, O. Scherman, *Renew. Sustain. Energy Rev.* **2017**, *68*, 333.
[5] S. Morsch, S. Lyon, S. R. Gibbon, *Prog. Org. Coat.* **2017**, *102*, 37.
[6] Y. Wang, W. Yan, M. Frey, M. V. Del Blanco, M. Schubert, M. Adobes-Vidal, E. Cabane, *Adv Sustain Syst* **2019**, *3*, 1.
[7] Japan Industrial Standards (JIS) K 5600–7–7 Testing methods for paints - Part 7: Long-period performance of film - Section 7: Accelerated weathering and exposure to artificial radiation (Exposure to filtered xenon-arc radiation), **2008**.
[8] B. Dou, Z. Zhu, E. Merkurjev, L. Ke, L. Chen, J. Jiang, Y. Zhu, J. Liu, B. Zhang, G.-W. Wei, *Chem. Rev.* **2023**, *123*, 8736.
[9] B. Lotter, S. Konde, J. Nguyen, M. Grau, M. Koch, P. Lenz, *Sci. Rep.* **2022**, *12*, 18840.
[10] N. Stavinski, V. Maheshkar, S. Thomas, K. Dantu, L. Velarde, *Environ. Sci. Adv.* **2023**, *2*, 1099.
[11] X. Chen, N. Kroell, M. Althaus, T. Pretz, R. Pomberger, K. Greiff, *Resour. Conserv. Recycl.* **2023**, *188*, 106719.
[12] N. S. Allen, M. J. Parker, C. J. Regan, R. B. Mcintyre, W. A. E. Dunk, *Polym. Degrad. Stab.* **1995**, *47*, 117.
[13] M. J. Melo, S. Bracci, M. Camaiti, O. Chiantore, F. Piacenti, *Polym. Degrad. Stab.* **1999**, *66*, 23.
[14] M. Vlad Cristea, B. Riedl, P. Blanchet, *Prog. Org. Coat.* **2010**, *69*, 432.
[15] F. Graziola, F. Girardi, R. Di Maggio, E. Callone, E. Miorin, M. Negri, K. Müller, S. Gross, *Prog. Org. Coat.* **2012**, *74*, 479.
[16] G. Gheno, R. Ganzerla, M. Bortoluzzi, R. Paganica, *Prog. Org. Coat.* **2016**, *101*, 90.
[17] J. Liu, Z. Li, L. Zhang, J. Hou, Z. Lu, P. Zhang, B. Wang, N. Jin, *Prog. Org. Coat.* **2019**, *136*, 105310.

[18] E. M. Dogan-Guner, S. Brownell, G. T. Schueneman, M. L. Shofner, J. C. Meredith, *Prog. Org. Coat.* **2021**, *150*, 105969.
[19] Q. Cao, I. Oluwoye, T. Pojtanabuntoeng, H. Farhat, M. Iannuzzi, *Prog. Org. Coat.* **2023**, *180*, 107544.
[20] A. Kitamura, M. Yamamoto, in *Inspection System, Inspection Method and Manufacturing Method of Inspection System*, (Ed.: M. Hojo) Dai Nippon Printing, Co., Ltd., Tokyo, Japan, **2022**, JP7130944B2.
[21] Agilent Technologies Inc, *Agilent 4300 Handheld FTIR Spectrometer*, Agilent Technologies, Santa Clara, CA **2023**.
[22] A. Ishikawa, Y. Kataoka, H. Ohki, K. Ka, T. Ito, T. Shimokawa, N. Hayashi, K. Magara, M. Kobayashi, T. Kanbayashi, M. Kiguchi, *Mokuzai Hozon (Wood Protect.)* **2019**, *45*, 68.
[23] H. Ohki, K. Ka, T. Ito, (Gen Gen Corporation), N. Hayashi, M. Kiguchi, Y. Kataoka, M. Kobayashi, T. Shimokawa, (Forestry and Forest Products Research Institute), JP6745747B2, Wood part paint, method of manufacturing wood part paint and method of applying wood part paint, **2020**.
[24] H. Kaneko, sample_program_4_10.py (for k-NN), https://github.com/hkaneko1985/python_data_analysis_ohmsha/blob/master/sample_program_4_10.py, (accessed: July, **2023**).
[25] H. Kaneko, sample_program_4_13.py (for DT), https://github.com/hkaneko1985/python_data_analysis_ohmsha/blob/master/sample_program_4_13.py, (accessed: July, **2023**).
[26] H. Kaneko, sample_program_4_14.py (for RF), https://github.com/hkaneko1985/python_data_analysis_ohmsha/blob/master/sample_program_4_14.py, (accessed: July, **2023**).
[27] H. Kaneko, sample_program_4_11.py (for SVM), https://github.com/hkaneko1985/python_data_analysis_ohmsha/blob/master/sample_program_4_11.py, (accessed: July, **2023**).
[28] H. Kaneko, in *Introduction to Data Analysis and Machine Learning with Python for Chemistry (in Japanese)*, Ohmsha, Ltd., Tokyo **2019**, p. 77.
[29] H. Kaneko, Dr. Hiromasa Kaneko's GitHub repository, https://github.com/hkaneko1985/python_data_analysis_ohmsha, (accessed: July, **2023**).
[30] S. Matsuoka, H. Kawamoto, S. Saka, *Polym. Degrad. Stab.* **2011**, *96*, 1242.
[31] T. Sato, R. Yamada, *J. Adhes. Soc. Japan* **2019**, *55*, 236.
[32] A. Kron, B. Stenberg, T. Reitberger, N. C. Billingham, *Polym. Degrad. Stab.* **1996**, *53*, 119.
[33] P. Gijsman, R. Fiorio, *Polym. Degrad. Stab.* **2023**, *208*, 110260.